

Geophysical Research Letters

RESEARCH LETTER

10.1029/2019GL086926

Key Points:

- We demonstrate data continuity of the GRACE and GRACE-FO missions for the world's glaciers and ice caps mass balance using independent data
- We report an acceleration in mass loss from the glaciers and ice caps during the GRACE/GRACE-FO time period
- Glaciers and ice caps contributed 281.5-Gt/yr mass loss over the last 17.33 yr or 13 mm of global sea level rise

Supporting Information:

- Supporting Information S1

Correspondence to:

E. Ciraci,
eciraci@uci.edu

Citation:

Ciraci, E., Velicogna, I., & Swenson, S. (2020). Continuity of the mass loss of the world's glaciers and ice caps from the GRACE and GRACE Follow-On missions. *Geophysical Research Letters*, 47, e2019GL086926. <https://doi.org/10.1029/2019GL086926>

Received 31 DEC 2019




Accepted 28 MAR 2020

Accepted article online 4 APR 2020

Corrected 14 JUN 2020

This article was corrected on 14 JUN 2020. See the end of the full text for details.

Continuity of the Mass Loss of the World's Glaciers and Ice Caps From the GRACE and GRACE Follow-On Missions

E. Ciraci¹ , I. Velicogna^{1,2} , and S. Swenson³ 

¹Department of Earth System Science, University of California Irvine, Irvine, CA, USA, ²Jet Propulsion Laboratory, California Institute of Technology, Pasadena, CA, USA, ³National Center for Atmospheric Research, Boulder, CO, USA

Abstract We use time series of time-variable gravity from the Gravitational Recovery and Climate Experiment (GRACE) and GRACE Follow-On (GRACE-FO) missions to evaluate the mass balance of the world's glaciers and ice caps (GIC) for the time period April 2002 to September 2019, excluding Antarctica and Greenland peripheral glaciers. We demonstrate continuity of the mass balance record across the GRACE/GRACE-FO data gap using independent data from the GMAO Modern-Era Retrospective Analysis for Research and Applications, Version 2 (MERRA-2) reanalysis. We report an average mass loss of 281.5 ± 30 Gt/yr, an acceleration of 50 ± 20 Gt/yr per decade, and a 13-mm cumulative sea level rise for the analyzed period. Seven regions dominate the mass loss, with the largest share from the Arctic: Alaska (72.5 ± 8 Gt/yr), Canadian Arctic Archipelago (73.0 ± 9 Gt/yr), Southern Andes (30.4 ± 13 Gt/yr), High Mountain Asia (HMA) (28.8 ± 11 Gt/yr), Russian Arctic (20.2 ± 6 Gt/yr), Iceland (15.9 ± 4 Gt/yr), and Svalbard (12.1 ± 4 Gt/yr). At the regional level, the analysis of acceleration is complicated by a strong interannual to decadal variability in mass balance that is well reproduced by the GRACE-calibrated MERRA-2 data.

Plain Language Summary We employ data from two consecutive spaceborne missions, Gravitational Recovery and Climate Experiment (GRACE) and GRACE Follow-On (GRACE-FO), that track changes in the gravity field of the Earth to quantify the mass loss of all of the GIC outside Greenland and Antarctica. We demonstrate data continuity across the 1 yr and a half data gap between the two missions using independent data from the NASA Global Modeling and Assimilation Office's Modern-Era Retrospective Analysis for Research and Applications, Version 2 (MERRA-2) reanalysis. We report an average mass loss of 281.5 Gt/yr, or 13 mm of sea level rise equivalent in 17.33 yr. The observational record reveals an acceleration in the rate of melt of glaciers and ice caps equivalent to adding an extra 0.14-mm sea level rise every decade.

1. Introduction

The world's glaciers and ice caps (GIC) contain an ice volume equivalent to a 0.4-m global sea level rise (SLR) (Vaughan et al., 2013). Although this contribution is small compared to Greenland (7 m) and Antarctica (57 m), the GIC were the largest contributor to global SLR in the 20th century. Available estimates suggest that during this time period, the GIC contributed between 0.13- and 0.6-mm/yr SLR (Cogley, 2009; Dowdeswell et al., 1997; Meier et al., 2007; Zuo & Oerlemans, 1997). Furthermore, SLR has accelerated during the last 50 yr (Church et al., 2011). Between 1993 and 2009, global SLR averaged 3 ± 0.4 mm/yr, with an acceleration of 0.8 ± 0.2 mm/yr per decade (Nerem et al., 2018). About 0.9 ± 0.4 mm/yr of the 3-mm/yr SLR has been attributed to the GIC alone (Cogley, 2009; Zuo & Oerlemans, 1997). Future projections indicate that glacier shrinkage will continue in the coming decades, hence continuing to affect SLR (Meier et al., 2007; Vaughan et al., 2013). In addition, runoff from the melting GIC has a major impact on regional hydrology and freshwater supply, especially in highly populated regions of Central Asia where it affects economic activities and political stability (Bolch et al., 2012; Koppes et al., 2015; Rupper et al., 2012). Defining consistent methodologies to monitor the state of GIC in these regions and reduce uncertainties regarding their specific mass loss are therefore critical not only to the science of SLR but also to the management of freshwater resources by local governments.

Presatellite era global assessments of the GIC were obtained principally through the interpolation of in situ measurements from local geodetic and glaciological techniques and glacier physical models

(Hirabayashi et al., 2010). In the former case, estimates were based on a sparse and irregularly distributed sampling of the GIC, therefore affected by large uncertainties. In the latter, physical models did not capture the processes driving the glacier mass change at a local scale with enough precision. Since then, numerous studies (Jacob et al., 2012; Tiwari et al., 2009) have demonstrated the practical use of satellite gravimetry data from the Gravitational Recovery and Climate Experiment (GRACE) to estimate the regional GIC ice mass changes. Jacob et al. (2012) calculated a GIC mass loss, outside Greenland and Antarctica, of 148 ± 30 Gt/yr during the period 2003–2010. Gardner et al. (2013) compared estimates from GRACE with estimates from satellite laser altimetry and extrapolations of in situ measurements to yield a mass loss of 215 ± 26 Gt/yr for 2003–2009. Rietbroek et al. (2016) reported a lower loss of 141 ± 26 Gt/yr for the time period 2002–2014 by applying a joint least squares inversion of GRACE, altimetry, and GPS data, while Schrama et al. (2014) found a loss of 162 ± 10 Gt/yr for the time period 2003–2013. Reager et al. (2016) estimated a larger 253 ± 35 Gt/yr mass loss for the time period 2002–2014 by mixing estimates from data sets covering different time periods: GRACE-based estimates (2002–2014) for Alaska, Canadian Archipelago, Iceland, Svalbard, and Russian Arctic; ICESat-derived estimates for High Mountain Asia (HMA) (Gardner et al., 2013); and the GMBAL estimates (2002–2012) (Cogley, 2009) for the remaining regions. More recently, however, Wouters and Moholdt (2019) estimated a loss of 199 ± 32 Gt/yr for the period 2002–2016. These studies used variable, often short time periods, which makes it difficult to compare the estimates and establish consensus estimates because the mass balance signal also exhibits a strong temporal variability. Similarly, these studies did not quantify the acceleration in mass loss of the GIC.

Here, we use the entire time series of GRACE observations, complemented by the early time series of the GRACE Follow-On (FO) mission, for a total time span of 17.33 yr spanning from April 2002 to September 2019. We use independent data from the Global Modeling and Assimilation Office (GMAO)'s Modern-Era Retrospective Analysis for Research and Applications, Version 2 (MERRA-2) to evaluate data continuity across the data gap between the two missions and determine how to fill the data gap. We discuss the evaluation of the mass balance of the GIC at the global and regional scales over the last 17.33 yr.

2. Data and Methodology

2.1. GRACE and GRACE-FO Data

We use 177 monthly GRACE and GRACE-FO Release-6 (RL06) spherical harmonic gravity solutions truncated to degree 60 from the Center for Space Research at the University of Texas (CSR) for the period April 2002 to September 2019 (Bettadpur, 2012; Tapley et al., 2004).

We employ monthly $C_{2,0}$ coefficients from satellite laser ranging provided by GSFC (Loomis et al., 2019) $C_{2,0}$ Stokes coefficients calculated using a time-variable gravity model derived from GRACE in the forward modeling of the SLR solution (Loomis et al., 2019), as opposed to the fixed background model used by Cheng and Ries (2017), which has been the standard oblateness solution up to now. We include degree-1 coefficients calculated following Sutterley and Velicogna (2019) self-consistent geocenter technique that includes self-attraction and loading effects. Sutterley and Velicogna (2019) allow a consistent processing of spherical harmonic fields (same C_{20} , C_{30} , GIA, and Love numbers), a higher degree truncation that has greater levels of agreement with our test synthetics, and a consistently buffered land-sea mask for geocenter calculation and sea level estimate. We remove the glacial isostatic adjustment (GIA), that is, the viscoelastic response by the solid Earth after the ice removal at the end of the last ice age, using Geruo et al. (2013) GIA model forced with ICE-6G loading history (Peltier et al., 2015). We remove the effects of post-Little Ice Age (LIA) isostatic rebound not included in the GIA model using Jacob et al. (2012) and Sørensen et al. (2017) corrections. We use the $C_{3,0}$ coefficients derived from satellite laser ranging provided by the Goddard Space Flight Center (GSFC) as a part of the GRACE TN-14 auxiliary data (Loomis et al., 2019). We evaluated the $C_{4,0}$ and $C_{5,0}$ Stokes coefficients and found that the GRACE/GRACE-FO coefficients have a satisfactory quality.

We calculate the glacier mass change time series using the least squares fit mascon approach of Jacob et al. (2012). Each mascon is an arbitrarily defined subregion composed of many small blocks defined on a regular $0.5^\circ \times 0.5^\circ$ latitude-longitude grid that covers the glacierized area. The distribution of mascon and $0.5^\circ \times 0.5^\circ$ cells is optimized to best follow the sixth Randolph Glacier Inventory Version 6.0 (RGIv6.0) (Arendt et al., 2014). We cover all GIC regions with a glacier area larger than 100 km^2 with one or more mascons. For each GIC region, we determine the sensitivity kernel, which is the sum of the sensitivity kernel for each mascon composing the region, that defines the sensitivity to the mass signal at every point inside the region as well

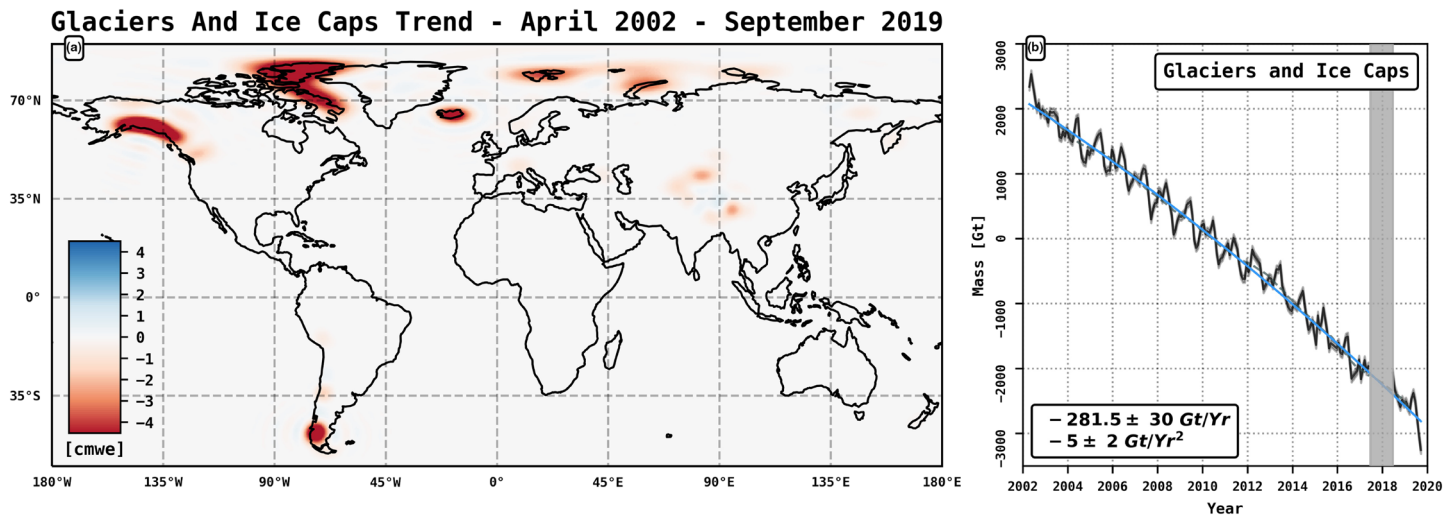


Figure 1. (a) Glaciers and ice caps (GIC) mass change derived from GRACE and GRACE-FO data for April 2002 to September 2019, in centimeter of water. (b) GRACE-derived ice mass time series for the GIC, with the best-fit quadratic trend (blue line) and monthly errors (light blue). Data filtered for the seasonal dependence using a 13-month window are shown (gray dashed line). Included are GRACE/GRACE-FO linear and quadratic trend estimates. Gray bar indicates the GRACE/GRACE-FO data gap.

as outside. If the mass change is uniform within each mascon, the mascon approach will recover the true mass change within the mascon and the signal from one mascon will not contaminate the solution for other mascons. For that reason, we include additional mascons to cover regions where no hydrology or ocean correction is available to minimize the leakage into the glacier mascon solution. For instance, there is no hydrological solution for Greenland and Antarctica; hence, we cover these areas with mascons. Conversely, it is not necessary to cover the entire world with mascons because if the number of mascon is too large, it produces noisy solutions (Jacob et al., 2012; Tiwari et al., 2009).

We evaluated several configurations of the mascon and the distribution of $0.5^\circ \times 0.5^\circ$ cells to determine which one provides the most localized kernel and minimizes the error of recovery of the mass change signal. We adjust the grid cells and mascons to ensure that all glacierized areas larger than 100 km^2 are fully included and not split on occasion (Figures 1 and 2 and supporting information Figure S1). If the signal is not uniform across one or more mascon, the signal could contaminate the solution for nearby mascons. To evaluate the leakage error, we use a Monte Carlo approach described below.

For each mascon, we calculate a set of Stokes coefficients up to degree 60, convert the mascons and the GRACE coefficients into mass, and smooth them employing a 150-km Gaussian function (Jacob et al., 2012). We simultaneously fit the mascon Stokes coefficients to the monthly GIA and hydrology corrected GRACE coefficients to obtain estimates of the average monthly mass variability for each mascon. We calculate the regional ice mass time series by summing the contributions from all mascons within the region. All trends are estimated with reference to November 2010.

The largest improvement in mascon configuration is for the HMA and Southern Andes (Figure S1). The Central Andes glaciers between 27°S and 31°S were only covered partially in Jacob et al. (2012) or not covered in Gardner et al. (2013). Even though this region includes small glaciers compared to the rest of the Andes, it is $2,800 \text{ km}^2$ in size. We cover them to estimate their mass change and avoid signal leakage to the surrounding ice-covered regions. Similarly, to avoid leakage from hydrological trends not included in the hydrology models used for correction, we compared model trends with GRACE. We find that effect of these errors is negligible except in the plains of Northern India, Pakistan, and Bangladesh, where significant human-induced groundwater withdrawal is not included in hydrological models. We cover this region with dedicated mascons (Rodell et al., 2009; Tiwari et al., 2009).

To isolate the GIC signal, the GRACE/GRACE-FO data are corrected for contamination by land hydrology using the average from two updated land surface models: (1) Version 5 of the Community Land Surface Model (CLM5) at 0.5° resolution (Oleson et al., 2013) and (2) Global Land Data Assimilation System 2.1 (GLDAS-2.1) model, Version NOAH-3.3, at 0.25° resolution (Rodell & Beaudoin, 2016). For both models,

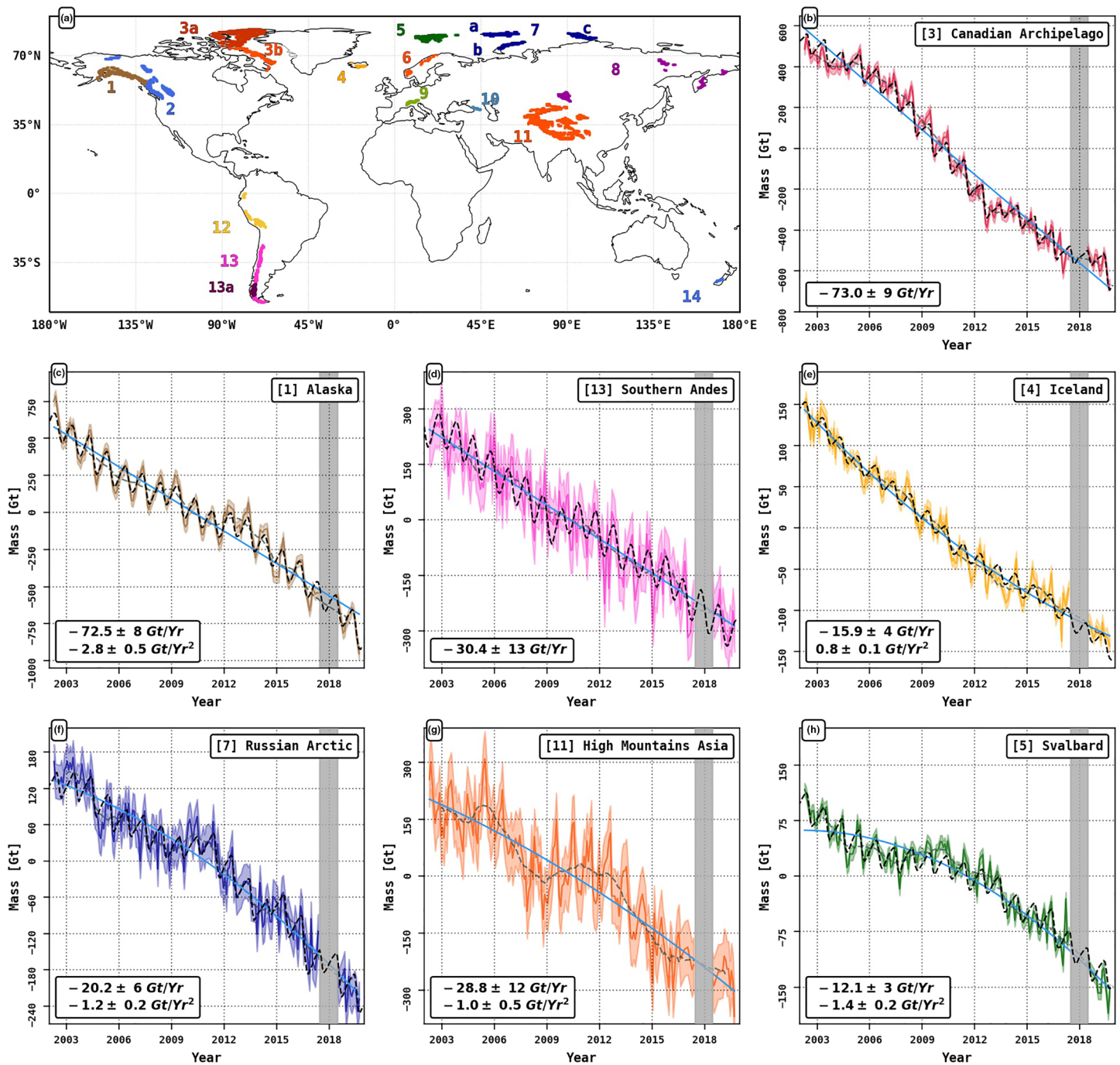


Figure 2. (a) Glaciers and ice caps locations from the Randolph Glacier Inventory Version 6.0 divided into 14 regions and subregions. GRACE-derived ice mass time series for the time period April 2002 to September 2019 for (b) [3] Canadian Archipelago, (c) [1] Alaska, (d) [13] Southern Andes, (e) [4] Iceland, (f) [7] Russian Arctic, (g) [11] High Mountain Asia, and (h) [5] Svalbard. Data filtered for the seasonal dependence using a 13-month window are shown (gray dashed line). Blue line is best-fit linear or quadratic trend. Light color band is monthly error. MERRA-2 data are black dashed line.

following Jacob et al. (2012) and Gardner et al. (2013), we zero out locations (glacier areas) where the rates of enhanced water storage are unrealistically high. We correct for the hydrology contribution by removing the average of the two models. The GLDAS-2.1 corrects for unnatural trends found in GLDAS-1 due to multiple switches of data sources over its records by using a consistent long term climatology and observational based forcing (Rui & Beaudoin, 2017). Within the glacier regions, the improvement in land hydrology is most significant for HMA where GLDAS-1 differs significantly from CLM5. We conserve mass at every step of

the inversion. When we remove the land hydrology or ocean signals, we redistribute mass over the land or ocean to conserve mass at every time step.

To determine if the mass change is accelerating during the analyzed period, we simultaneously fit an annual and a semiannual signal, a quadratic trend, a linear trend, and a constant. To be conservative in our estimate of the regression error, we do not make any assumption about the size of the error affecting the GRACE/GRACE-FO monthly estimates. We only consider an acceleration if the signal is significant at the 2σ confidence level. To determine if the quadratic model is statistically more significant than the linear one, we calculate the best fitting linear trend and associated error (2σ confidence level). We use a variant of the Akaike information criterion for use with small sample-sized data sets (AIC_c) to compare the quadratic and linear model fits. We report an acceleration only when the AIC_c indicates that the improvement in data fitting of the quadratic model is significant at the 99% confidence level compared to the linear fit (Burnham & Anderson, 2002; Raftery, 1995). To evaluate the percentage variance of the observed signal explained by the model fit, we calculate the adjusted coefficient of determination R^2_{adj} (Weisberg, 2005) for the linear and quadratic models. The R^2_{adj} provides a measure of the percentage variance of the observed signal explained by a regression model. To determine at what statistical level the difference between the R^2_{adj} is significant, we use an F test (Berry et al., 1985).

The uncertainty in glacier mass loss for each regions includes the quadratic sum of the GRACE/GRACE-FO measurement errors, the GIA and LIA errors, the uncertainty associated with the hydrological correction calculated as the average of GLDAS-2.1 and CLM5, the error in the ocean mass estimate, the leakage error because the mass change is not uniform within each mascon, and the statistical uncertainty of the time series regression (Table S1). The GRACE measurement errors are calculated following Velicogna and Wahr (2013) as the root-mean-square (RMS) of the residual between the GRACE time series and the time series after a high-pass filter that removes frequencies of once and twice per year is applied. This estimate is conservative because intraannual variations in the signal are interpreted as errors. The GIA, LIA, and hydrology correction errors are as in Jacob et al. (2012) and Gardner et al. (2013). The contribution of ocean mass change to monthly gravity anomaly is evaluated and removed by the processing centers prior to computing gravity field solutions using the Ocean Model for Circulation and Tides (OMCT) ocean general circulation model (Dobslaw et al., 2013). Following Velicogna and Wahr (2013), we assume that the error is equal to the correction.

To evaluate the leakage error introduced by assuming a uniform mass distribution within each mascon, we use a Monte Carlo simulation. For each mascon, we generate 10,000 mass distributions by spreading the recovered monthly mass changes nonuniformly within the mascon using pseudorandom weights extracted from a Gaussian distribution with unit standard deviation and zero mean. We convert these 10,000 mass distributions into harmonics, truncated to degree and order 60, apply the mascon fit to each distribution, and calculate the difference between original mass loss and that obtained with the randomly generated distributions. The leakage error is equal to two times the standard deviation of the 10,000 differences.

2.2. MERRA-2 SMB Data

We calculate monthly values of the glacier surface mass balance (SMB) using outputs from the NASA MERRA-2 (Gelaro et al., 2017) provided for the time period 1980 to 2019 at a spatial resolution of $0.5^\circ \times 0.625^\circ$ (50 km). MERRA-2 is the latest atmospheric reanalysis of the modern satellite era produced by NASA's GMAO based on Version 5.12.4 of the GEOS atmospheric data assimilation system. MERRA-2 replaces MERRA (Rienecker et al., 2011), which suffered from unphysical jumps and trends in precipitation in response to changes in the observing system, biases and imbalances in certain atmospheric and land surface hydrological quantities, a poor representation of the upper stratosphere, and limited capability to incorporate new-generation satellite observations (Gelaro et al., 2017). GEOS-5.12.4 uses an improved snow hydrology model with densification, melt water runoff, percolation, refreezing, and surface albedo, and a 15-layer ice column for modeling heat transfer below the snow-ice interface (Cullather et al., 2014). The regions with represented land ice processed are identified by the fractional land ice variable "FRLANDICE" in the constant model parameter collection available (at gmao.gsfc.nasa.gov/reanalysis/MERRA-2/) including Alaska, Western Canada, Southern Andes, Canadian Arctic Archipelago (CAA), Iceland, Russian Arctic, Svalbard, Central Europe, Western Himalaya, Himalaya, and New Zealand. MERRA-2 does cover HMA. In Baffin Island, Iceland, Novaya Zemlya, and Severnaya Zemlya, the model overestimates the glacier area by more than a factor 2 with respect to RGIv6.0 (Arendt et al., 2014). In these cases, we design ad hoc

Table 1

Glaciers and Ice Caps (GIC) Mass Balance in Gt/yr ($Gt = 10^{12}$ kg) and Acceleration in Gt/yr^2 from April 2002 to September 2019 Divided Into 14 Regions (Figure 1)

Glacier region	Mass balance [Gt/yr]	Acceleration [Gt/yr ²]	$R^2_{adj}(L)$ [%]	$R^2_{adj}(Q)$ [%]	F test [%]	AIC_c [Q/L]
1. Alaska	-72.5 ± 8	-2.8 ± 0.5	95.8	96.6	Q at 99.9	Q
2. Western Canada/U.S.	-15.1 ± 11	-1.0 ± 0.3	76.4	78.4	Q at 99.9	Q
3. Canadian Archipelago	-73.0 ± 9	—	96.4	96.4	—	L
3a. Arctic Canada North	-41.2 ± 7	—	95.3	95.3	—	L
3b. Arctic Canada South	-31.8 ± 5	—	96.0	96.0	—	L
4. Iceland	-15.9 ± 4	0.8 ± 0.1	96.6	97.7	Q at 99.9	Q
5. Svalbard	-12.1 ± 3	-1.4 ± 0.2	85.3	91.4	Q at 99.9	Q
6. Scandinavia	-1.7 ± 5	-0.4 ± 0.1	37.6	40.6	Q at 99.9	Q
7. Russian Arctic	-20.2 ± 6	-1.2 ± 0.2	91.5	93.1	Q at 99.9	Q
7a. Franz Joseph Land	-5.5 ± 3	-0.4 ± 0.1	83.4	85.8	Q at 99.9	Q
7b. Novaya Zemlya	-10.8 ± 3	-0.6 ± 0.1	89.2	90.6	Q at 99.9	Q
7c. Severnaya Zemlya	-3.8 ± 2	—	81.6	82.0	Q at 96.9	L
8. North Asia	-2.9 ± 7	—	41.3	41.0	—	L
9. Central Europe	-3.0 ± 3	—	61.1	61.1	—	L
10. Caucasus Middle East	-1.8 ± 3	-0.25 ± 0.1	25.7	29.5	Q at 99.9	Q
11. High Mountain Asia	-28.8 ± 12	-1.0 ± 0.5	84.4	85.0	Q at 97.7	Q
11a. East and West Tien Shan	-11.9 ± 3	-0.3 ± 0.1	93.0	93.5	Q at 99.9	Q
11b. Hindu Kush, Karakoram, West Kunlun, Pamir, and Hissar Alay	-5.2 ± 4	-0.8 ± 0.2	55.1	59.8	Q at 99.9	Q
11c. Himalaya, Hengduan Shan, and South and East Tibet	-12.2 ± 7	—	29.9	30.5	—	L
11d. East Kunlun, Inner Tibet, and Qilian Shan	2.0 ± 4	—	76.0	76.3	Q at 91.6	L
12. Low Latitudes	-1.6 ± 6	0.8 ± 0.2	12.7	19.1	Q at 99.9	Q
13. Southern Andes	-30.4 ± 13	—	90.6	90.6	—	L
13a. Northern and Southern Patagonian Ice Fields	-28.0 ± 6	-0.4 ± 0.2	98.0	98.4	Q at 99.9	Q
14. New Zealand	-0.7 ± 3	—	6.3	7.1	Q at 88.8	L
Total	-281.5 ± 30	-5 ± 2	95.1	97.3	Q at 99.9	Q

Note. $R^2_{adj}(L)$ and $R^2_{adj}(Q)$ (in %) are the R^2 adjusted for linear and quadratic models, respectively. F test shows at what statistical level the improvement in explained variance of the more complex model is not occurring by chance. The Akaike information criterion, AIC_c , indicates if the linear (L) or quadratic (Q) model best fits the signal.

ice regional glacier masks based on RGIv6.0. We calculate monthly SMB values as net precipitation minus evaporation and runoff. Minor ice wastage components, for example, sublimation and wind erosion, are not included (Bosilovich, 2015).

We compare MERRA-2 SMB with GRACE data assuming that changes in ice discharge from marine-terminating glaciers are negligible, which is a reasonable assumption for most regions. First, we calibrate the SMB data with GRACE data over the GRACE period. To do so, we compare the trends in mass change, dM/dt (where M is the mass and t is the time) derived from SMB and GRACE. The differences in trend represent uncertainties in GIA correction for GRACE (a constant dM/dt) and uncertainties in absolute SMB for MERRA-2 (a constant dM/dt) (Lang et al., 2015; Lenaerts et al., 2013) (Table S2). We adjust the SMB time series with this correction and compare the adjusted SMB time series with GRACE-FO data.

3. Results

During 2002–2019, the GIC total mass loss, outside Greenland and Antarctica, averages 281.5 ± 30 Gt/yr, with a statistically significant acceleration in loss of 5 ± 2 Gt/yr², or 50 ± 20 Gt/yr per decade (Figure 1). The total mass loss in 17.33 yr is 4,540 Gt, or 13 mm of global sea level equivalent. The R^2_{adj} for the entire global GIC time series is 97.3% ($p < 0.001$) for the quadratic model, and the difference in fit skill between the quadratic and linear models of 2.2% is significant at the 99.9% confidence level, that is, we detect a significant acceleration in mass loss over that time period.

Time series for the largest contributors (Figure 2) and the remaining regions (Figures S2–S4) of mass change and acceleration (Table 1) show that seven regions covering 94% of the total GIC area account for 90% of the total loss: (1) Alaska, (2) CAA, (3) Southern Andes, (4) HMA, (5) Russian Arctic, (6) Iceland, and (7) Svalbard. The Arctic alone, with 65% of the GIC in area, accounts for 69% of the mass loss, with Alaska, CAA, Russian Arctic, Iceland, and Svalbard (Table 1).

The comparison of GRACE/GRACE-FO data with the MERRA-2 data shows an excellent agreement across the data gap at the regional level, except for HMA, which is not included in MERRA-2. The small values of adjustments needed to match MERRA-2 with GRACE/GRACE-FO (Table S1) are indicative of both the quality of the GRACE processing and the high reliability of the MERRA-2 data. Hence, we can confidently fill the data gap between missions using the MERRA-2 data. The MERRA-2 data reproduce the trend, seasonal variability, and interannual variability within a few percent of the total signal. The RMS error between GRACE and MERRA-2 is 3% (Alaska, CAA), 5% (Svalbard), 6% (Russian Arctic), 10% (Southern Andes), and 14% (Northwest America) of the signal.

Alaska exhibits the largest mass loss of all regions with 72.5 ± 8 Gt/yr, a statistically significant acceleration of 28 ± 5 Gt/yr per decade. CAA is the second with a mass loss of 73 ± 11 Gt/yr but no statistically significant acceleration. The mass loss for northern CAA (Figure S2a) is 41.2 ± 7 versus 31.8 ± 5 Gt/yr for the southern part (Figure S2b). Over 2003–2009, our estimate of 54 ± 13 Gt/yr (Table S2) agrees with GRACE RL05 58 ± 9 Gt/yr from Gardner et al. (2013) and their estimate from multiple techniques of 60 ± 6 Gt/yr. For 2003–2012, our estimate of 69 ± 9 Gt/yr agrees with 69 ± 6 Gt/yr from Lenaerts et al. (2013). For 2003–2014, our results for CAA and Alaska agree with Harig and Simons (2016). For Alaska, our mass loss is 51.5 ± 7 versus 40 ± 5 Gt/yr. For Ellesmere Island and Baffin Island, we find 45.5 ± 9 and 33.5 ± 6 Gt/yr, respectively, versus 38 ± 2 and 22 ± 2 Gt/yr, respectively. They use the GIA correction of Paulson et al. (2007), do not include LIA correction, use the CSR CL05 GRACE solutions, and use a different configuration for Alaska.

Outside the Arctic, the Southern Andes (Figure 2d) exhibits the third largest loss with 30.4 ± 13 Gt/yr, almost entirely from the Northern and Southern Patagonian Ice Fields (NPI and SPI) with 28 ± 6 Gt/yr (Figure S2) and a significant acceleration of 4 Gt/yr per decade. The R^2_{adj} is 98.0% ($p < 0.001$) and 98.4% ($p < 0.001$), respectively, for the quadratic and linear fits for NPI and SPI. The mass loss of SPI during 2002–2012 agrees with Willis et al. (2012).

The HMA has the fourth largest loss with 28.8 ± 12 Gt/yr and an acceleration of 10 ± 5 Gt/yr per decade (Figure 1g). The R^2_{adj} is 85.0% ($p < 0.001$) for quadratic versus 84.4% ($p < 0.001$) for linear, and the difference is significant at the 99.9% confidence level. We divide the HMA into four subregions based on precipitation and compatibility with the GRACE spatial resolution: (11a) the Tien Shan; (11b) Karakoram, Hindu Kush, Kunlun, Pamir, and Hissar Alay; (11c) the Qilian Shan, Inner Tibet, and E Kunlun; and (11d) Himalaya (West, Central, and East) and South and East Tibet and Hengduan Shan (Figure S4). The largest signal comes from Region 11d with a mass loss of 12.2 ± 7 Gt/yr, followed by Region 11a with a loss of 11.9 ± 3 Gt/yr and an acceleration in loss of 0.3 ± 0.1 Gt/yr², Region 11b with a loss of 5.2 ± 4 Gt/yr and an acceleration of 0.8 ± 0.2 Gt/yr². These results agree with Brun et al. (2017) for 2000–2016. In Region 11c, however, we find a mass gain of 2.0 ± 4 Gt/yr inconsistent with the 0.8 Gt/yr loss from Brun et al. (2017). The HMA region displays a strong interannual variability in mass balance, which explains why the R^2_{adj} is lower than in most other regions, dominated by the western portion of the HMA.

The Russian Arctic (Figure 1f) has the fifth largest loss with 20.2 ± 6 Gt/yr and an acceleration of 10 ± 2 Gt/yr per decade. The quadratic R^2_{adj} is 93.1% ($p < 0.001$) versus 91.5% ($p < 0.001$) for quadratic and linear, and the improvement of the quadratic fit is significant at the 99.9% confidence level. We find a mass loss of 5.5 ± 3 Gt/yr for Franz Joseph Land, 10.8 ± 4 Gt/yr for Novaya Zemlya, and 3.8 ± 3 Gt/yr for Severnaya Zemlya (Figure S2), and an acceleration in loss of 0.4 ± 0.1 Gt/yr² for Franz Joseph Land and 0.6 ± 0.1 Gt/yr² for Novaya Zemlya, but none for Severnaya Zemlya.

Iceland (Figure 2e) has the sixth largest loss with 15.9 ± 4 Gt/yr, with a negative acceleration of -8 ± 1 Gt/yr per decade. The R^2_{adj} is 97.7% ($p < 0.001$) for the quadratic versus 96.6% ($p < 0.001$) for the linear, and the difference is significant at the 99.9% confidence level. Svalbard has the seventh largest loss, with 12.1 ± 3 Gt/yr, and an acceleration of 13 ± 2 Gt/yr per decade (Figure 2h). R^2_{adj} is 91.4% ($p < 0.001$) for the quadratic versus 85.3% ($p < 0.001$) for the linear, and the difference is significant at the 99.9% confidence level.

For the remaining small regions of Central Europe, Caucasus, Central America, North Asia, Scandinavia, and Low Latitudes, which represent 6% of the GIC area, the uncertainty in mass loss is larger, but their contribution to the total mass loss of GIC is less than 10%.

4. Discussion

The continuity in trend of the GRACE and GRACE-FO time series is a testimony of the data quality and calibration of both missions with no period of overlap. Data continuity is manifest at the GIC and region scales and best illustrated using independent MERRA-2 data. We find no bias in the GRACE and GRACE-FO time series from the continental to the regional levels, in both hemispheres, which is indicative of the high quality of the GRACE processing (Tapley et al., 2019). The small adjustments in trend between MERRA-2 and GRACE/GRACE-FO indicate that we can confidently fill the data gap with MERRA-2 data, except for HMA.

The mass balance of the GIC is dominated by SMB processes, as is well known in the case of Alaska and the Canadian Archipelago (Larsen et al., 2015; Millan et al., 2017). Exceptions for which contribution from ice dynamics are significant include Svalbard and the Russian Arctic (Carr et al., 2017; Ciraci et al., 2018; Dunse et al., 2015; Lang et al., 2015; Matsuo & Heki, 2013; McMillan et al., 2014; Melkonian et al., 2016), but over the short time periods such as the GRACE/GRACE-FO data gap, including changes in ice dynamics of these regions would not significantly alter our results for filling the data gap because the additional mass change caused by ice dynamics would be nearly constant and hence already absorbed by the calibration of the MERRA-2 data.

Our GIC estimates for 2003–2009 agree with Gardner et al. (2013) (Figure S1 and Table S2), except for the Southern Andes where we use an updated inventory. Our errors for HMA are also two times smaller because of improved hydrological corrections (Table S2). Our mass loss estimates are higher than Rietbroek et al. (2016) for 2002–2014, but they reported an agreement with Jacob et al. (2012) for 2003–2010 despite an increase in mass loss after 2010. Our GIC loss agree with Reager et al. (2016) over the same period. We find higher mass losses than Schrama et al. (2014) for 2003–2013 (142.7 ± 7.8 Gt/yr), with the largest difference in Alaska and the Southern Andes where we agree with Gardner et al. (2013) and Reager et al. (2016). We attribute most of these differences to differences in time period and small variations in methodology and corrections.

Our longer GRACE/GRACE-FO time series enables a robust analysis of the interannual variability in mass balance and a statistically significant detection of an acceleration in mass loss of the GIC. At the regional level, the interannual to decadal variability of the signal is pronounced and makes it more difficult to detect acceleration.

In the CAA, the mass loss increase after 2005 was due to an increase in runoff (Gardner et al., 2011; Lenaerts et al., 2013; Mortimer et al., 2018). Regional mean summer temperature over the CAA for 2002–2019 from monthly observations by the Climate Research Unit Time Series Version 4.01 (CRU-TS) (Harris et al., 2014) indicate that 8 yr after 2005 (2007–2012 and 2015–2016) had a mean temperature above the 2002–2016 mean. After 2016, colder conditions led to a pause in the increase in mass loss until year 2019 where the region experienced a 200-Gt mass loss (Figure 2). Key factors for the exceptional loss of 2019 were the persistence of anticyclonic conditions over the summer, promoting high snow and ice melt, combined with low precipitation of snow in the previous winter. A low cloud cover in the north induced high loss even though the air temperature was only 1 to 2 °C warmer than the average for 1981–2010 (Tedesco & Fettweis, 2020).

In the Russian Arctic, we find a higher loss than in Moholdt et al. (2012) for 2003–2009, which is more balanced between regions: 5.5 ± 3 Gt/yr for Franz Joseph Land (25% of the total loss, 4 times higher), 10.8 ± 4 Gt/yr for Novaya Zemlya (53%), and 3.8 ± 3 Gt/yr for Severnaya Zemlya (21%, 2 times higher). Melkonian et al. (2016) noted that the mass loss for Novaya Zemlya in 2012–2014 (8.8 ± 2 Gt/yr) was higher than the mass loss over the last 65 yr (0.5 Gt/yr) because of warmer air temperatures (Zhao et al., 2014) and enhanced thinning of marine-terminating glaciers (Carr et al., 2017; Ciraci et al., 2018; Melkonian et al., 2016).

In Svalbard, the increase in GRACE-derived mass loss after 2010 has been attributed to enhanced ice discharge and reduced SMB (Lang et al., 2015; Matsuo & Heki, 2013; McMillan et al., 2014). McMillan et al. (2014) reported an increase in glacier thinning after 2009 for the marine-based sectors of Austfonna, followed by an exceptionally high loss after 2012 during a major increase in ice velocity (Dunse et al., 2015).

Record runoff levels were observed in 2013 due to warm summer air temperatures caused by a southwesterly flow over Svalbard (Lang et al., 2015). The increase in loss has persisted up to 2019.

In Iceland, we observe a slowdown in mass loss after 2011 until 2019. The mean summer temperature by the CRU-TS shows that the decrease in mass loss in 2011–2016 was due to colder summer temperatures compared to the 2002–2011 mean, consistent with Foresta et al. (2016). The high interannual variability of the Icelandic mass balance reflects its sensitivity to temperature and precipitation (Aðalgeirsdóttir et al., 2006; Björnsson et al., 2013; De Woul & Hock, 2005). In 2010, we observe 50-Gt loss that coincides with the large melt event caused by the Eyjafjallajökull eruption (Björnsson et al., 2013). In 2019, we observe a large drop in mass.

With a glacier area of 97,606 km², HMA is the largest ice-covered region outside the Arctic. The acceleration of 1 ± 0.5 Gt/yr² is due to Regions 11a and 11b, whereas Regions 11a and 11c control the majority of the loss (11.9 ± 3 and 12.2 ± 7 Gt/yr). The acceleration in mass loss in Regions 11a and 11b is driven by a large interannual variability in precipitation, which is more apparent after year 2009 (Figure S4) and reflects an influx of solid precipitation from the Mediterranean Sea during the winter season (Yao et al., 2012; Zhan et al., 2017). The interannual variability in mass loss of HMA has been linked to the interaction between large-scale atmospheric circulation patterns and local topography determining regional precipitation regimes and atmospheric temperatures (Aizen et al., 2001; Yao et al., 2012), which is manifest in the western Regions 11a and 11b (Figures S4b and S4c).

5. Conclusions

We employ the latest glacier inventories, hydrological corrections, complete time series, and optimized mascons minimizing leakage to extend the mass budget of the world's GIC using the entire GRACE and GRACE-FO mission data. We demonstrate the consistency of the two missions using independent data from the GMAO MERRA-2 reanalysis, at the global and regional scales, in both hemispheres. The data gap between GRACE and GRACE-FO can be confidently filled with MERRA-2 data to provide a continuous record of mass balance. Over the 17.33-yr period, we detect an average mass loss of 281.5 ± 30 Gt/yr, equivalent to 13 ± 2 mm of global SLR from the GIC. We detect an acceleration in mass loss over the time period and note that the mass loss is dominated by seven regions, five of which are from the Arctic.

Acknowledgments

This work was performed at the University of California Irvine and at Caltech's Jet Propulsion Laboratory; it was supported by the National Aeronautics and Space Administration's Cryosphere, Understanding Changes in High Mountain Asia, GRACE, and GRACE-FO programs. GRACE data are available at the website (grace.jpl.nasa.gov). MERRA-2 data are available at the website (<https://gmao.gsfc.nasa.gov/reanalysis/MERRA-2/>). Data to reproduce the figures are available at the website (ess.uci.edu/~velicogna/GIC-grace-grace-fo-2020.php). We thank Jennifer Boning and another anonymous reviewer.

References

- Aðalgeirsdóttir, G., Jóhannesson, T., Björnsson, H., Pálsson, F., & Sigurðsson, O. (2006). Response of Hofsjökull and southern Vatnajökull, Iceland, to climate change. *Journal of Geophysical Research*, 111, F03001. <https://doi.org/10.1029/2005JF000388>
- Aizen, E. M., Aizen, V. B., Melack, J. M., Nakamura, T., & Ohta, T. (2001). Precipitation and atmospheric circulation patterns at mid-latitudes of Asia. *International Journal of Climatology: A Journal of the Royal Meteorological Society*, 21(5), 535–556.
- Arendt, A. A., Bliss, A., Bolch, T., Cogley, J. G., Gardner, A. S., & Randolph, C. (2014). The Randolph Glacier Inventory: A globally complete inventory of glaciers. *Journal of Glaciology*, 60, 537–552. <https://doi.org/10.3189/2014JoG13176>
- Berry, W. D., Berry, W. D., Feldman, S., & Stanley Feldman, D. (1985). Multiple regression in practice. (No. 50). Sage.
- Bettadpur, S. (2012). *UTCSR level-2 processing standards document, technical report GRACE*. Austin, Texas: Center for Space Research, University of Texas.
- Björnsson, H., Pálsson, F., Gudmundsson, S., Magnússon, E., Adalgeirsdóttir, G., Jóhannesson, T., & Thorsteinsson, T. (2013). Contribution of Icelandic ice caps to sea level rise: Trends and variability since the Little Ice Age. *Geophysical Research Letters*, 40, 1546–1550. <https://doi.org/10.1002/grl.50278>
- Bolch, T., Kulkarni, A., Kääb, A., Huggel, C., Paul, F., Cogley, J. G., & Stoffel, M. (2012). The state and fate of Himalayan glaciers. *Science*, 336(6079), 310–314. <https://doi.org/10.1126/science.1215828>
- Bosilovich, M. G. (2015). *MERRA-2: Initial evaluation of the climate*. Greenbelt, MD: National Aeronautics and Space Administration, Goddard Space Flight Center.
- Brun, F., Berthier, E., Wagnon, P., Kääb, A., & Treichler, D. (2017). A spatially resolved estimate of High Mountain Asia glacier mass balances from 2000 to 2016. *Nature Geoscience*, 10, 668–673. <https://doi.org/10.1038/ngeo2999>
- Burnham, K. P., & Anderson, D. R. (2002). *Model selection and multimodel inference*. New York, 175 Fifth Avenue, New York, NY: Springer-Verlag.
- Carr, J. R., Bell, H., Killick, R., & Holt, T. (2017). Exceptional retreat of Novaya Zemlya's marine-terminating outlet glaciers between 2000 and 2013. *The Cryosphere*, 11(5), 2149–2174. <https://doi.org/10.5194/tc-11-2149-2017>
- Cheng, M., & Ries, J. (2017). The unexpected signal in GRACE estimates of C_{20} . *Journal of Geodesy*, 91(8), 897–914.
- Church, J. A., White, N. J., Konikow, L. F., Domingues, C. M., Cogley, J. G., Rignot, E., & Velicogna, I. (2011). Revisiting the Earth's sea-level and energy budgets from 1961 to 2008. *Geophysical Research Letters*, 38, L18601. <https://doi.org/10.1029/2011GL048794>
- Ciraci, E., Velicogna, I., & Sutterley, T. (2018). Mass balance of Novaya Zemlya Archipelago, Russian High Arctic, using time-variable gravity from GRACE and altimetry data from ICESat and CryoSat-2. *Remote Sensing*, 10(11), 1817.
- Cogley, J. G. (2009). Geodetic and direct mass-balance measurements: Comparison and joint analysis. *Annals of Glaciology*, 50(50), 96–100. <https://doi.org/10.3189/172756409787769744>
- Cullather, R. I., Nowicki, S. M., Zhao, B., & Suarez, M. J. (2014). Evaluation of the surface representation of the Greenland Ice Sheet in a general circulation model. *Journal of Climate*, 27(13), 4835–4856.

- De Woul, M., & Hock, R. (2005). Static mass-balance sensitivity of Arctic glaciers and ice caps using a degree-day approach. *Annals of Glaciology*, 42(Table 1), 217–224. <https://doi.org/10.3189/172756405781813096>
- Dobslaw, H., Flechtner, F., Bergmann-Wolf, I., Dahle, C., Dill, R., Esselborn, S., & Thomas, M. (2013). Simulating high-frequency atmosphere-ocean mass variability for dealiasing of satellite gravity observations: AOD1B RL05. *Journal of Geophysical Research: Oceans*, 118, 3704–3711. <https://doi.org/10.1002/jgrc.20271>
- Dowdeswell, J. A., Hagen, J. O., Björnsson, H., Glazovsky, A. F., Harrison, W. D., Holmlund, P., & Thomas, R. H. (1997). The mass balance of circum-Arctic glaciers and recent climate change. *Quaternary Research*, 48(1), 1–14. <https://doi.org/10.1006/qres.1997.1900>
- Dunse, T., Schellenberger, T., Hagen, J. O., Käb, A., Schuler, T. V., & Reijmer, C. H. (2015). Glacier-surge mechanisms promoted by a hydro-thermodynamic feedback to summer melt. *The Cryosphere*, 9(1), 197–215. <https://doi.org/10.5194/tc-9-197-2015>
- Foresta, L., Gourmelen, N., Pálsson, F., Nienow, P., Björnsson, H., & Shepherd, A. (2016). Surface elevation change and mass balance of Icelandic ice caps derived from swath mode CryoSat-2 altimetry. *Geophysical Research Letters*, 43, 2016GL071485. <https://doi.org/10.1002/2016GL071485>
- Gardner, A. S., Moholdt, G., Cogley, J. G., Wouters, B., Arendt, A. A., Wahr, J., & Paul, F. (2013). A reconciled estimate of glacier contributions to sea level rise: 2003 to 2009. *Science*, 340(6134), 852–857. <https://doi.org/10.1126/science.1234532>
- Gardner, A. S., Moholdt, G., Wouters, B., Wolken, G. J., Burgess, D. O., Sharp, M. J., & Labine, C. (2011). Sharply increased mass loss from glaciers and ice caps in the Canadian Arctic Archipelago. *Nature*, 473(7347), 357–360. <https://doi.org/10.1038/nature10089>
- Gelaro, R., McCarty, W., Suárez, M. J., Todling, R., Molod, A., Takacs, L., et al. (2017). The Modern-Era Retrospective Analysis for Research and Applications, Version 2 (MERRA-2). *Journal of Climate*, 30(14), 5419–5454. <https://doi.org/10.1175/JCLI-D-16-0758.1>
- Geruo, A., Wahr, J., & Zhong, S. (2013). Computations of the viscoelastic response of a 3-D compressible Earth to surface loading: An application to glacial isostatic adjustment in Antarctica and Canada. *Geophysical Journal International*, 192(2), 557–572. <https://doi.org/10.1093/gji/ggs030>
- Harig, C., & Simons, F. J. (2016). Ice mass loss in Greenland, the Gulf of Alaska, and the Canadian Archipelago: Seasonal cycles and decadal trends. *Geophysical Research Letters*, 43, 3150–3159. <https://doi.org/10.1002/2016GL067759>
- Harris, I., Jones, P., Osborn, T., & Lister, D. (2014). Updated high-resolution grids of monthly climatic observations—The CRU TS3.10 Dataset. *International Journal of Climatology*, 34, 623–642.
- Hirabayashi, Y., Döll, P., & Kanae, S. (2010). Global-scale modeling of glacier mass balances for water resources assessments: Glacier mass changes between 1948 and 2006. *Journal of Hydrology*, 390(3), 245–256. <https://doi.org/10.1016/j.jhydrol.2010.07.001>
- Jacob, T., Wahr, J., Pfeffer, W. T., & Swenson, S. (2012). Recent contributions of glaciers and ice caps to sea level rise. *Nature*, 482(7386), 514–518. <https://doi.org/10.1038/nature10847>
- Koppes, M., Rupper, S., Asay, M., & Winter-Billington, A. (2015). Sensitivity of glacier runoff projections to baseline climate data in the Indus River basin. *Frontiers in Earth Science*, 3, 59. <https://doi.org/10.3389/feart.2015.00059>
- Lang, C., Fettweis, X., & Erpicum, M. (2015). Stable climate and surface mass balance in Svalbard over 1979–2013 despite the Arctic warming. *The Cryosphere*, 9(1), 83–101. <https://doi.org/10.5194/tc-9-83-2015>
- Larsen, C. F., Burgess, E., Arendt, A. A., O'Neel, S., Johnson, A. J., & Kienholz, C. (2015). Surface melt dominates Alaska glacier mass balance. *Geophysical Research Letters*, 42, 5902–5908. <https://doi.org/10.1002/2015GL064349>
- Lenaerts, J. T. M., van Angelen, J. H., van den Broeke, M. R., Gardner, A. S., Wouters, B., & van Meijgaard, E. (2013). Irreversible mass loss of Canadian Arctic Archipelago glaciers. *Geophysical Research Letters*, 40, 870–874. <https://doi.org/10.1002/grl.50214>
- Loomis, B. D., Rachlin, K. E., & Luthcke, S. B. (2019). Improved Earth oblateness rate reveals increased ice sheet losses and mass-driven sea level rise. *Geophysical Research Letters*, 46, 6910–6917. <https://doi.org/10.1029/2019GL082929>
- Matsuo, K., & Heki, K. (2013). Current ice loss in small glacier systems of the Arctic Islands (Iceland, Svalbard, and the Russian High Arctic) from satellite gravimetry. *Terrestrial, Atmospheric and Oceanic Sciences*, 24(4–1), 657–670. [https://doi.org/10.3319/TAO.2013.02.22.01\(TibXS\)](https://doi.org/10.3319/TAO.2013.02.22.01(TibXS))
- McMillan, M., Shepherd, A., Gourmelen, N., Dehecq, A., Leeson, A., Ridout, A., & Strozzi, T. (2014). Rapid dynamic activation of a marine-based Arctic ice cap. *Geophysical Research Letters*, 41, 8902–8909. <https://doi.org/10.1002/2014GL062255>
- Meier, M. F., Dyurgerov, M. B., Rick, U. K., O'Neel, S., Pfeffer, W. T., Anderson, R. S., & Glazovsky, A. F. (2007). Glaciers dominate eustatic sea-level rise in the 21st century. *Science*, 317(5841), 1064–1067. <https://doi.org/10.1126/science.1143906>
- Melkonian, A. K., Willis, M. J., Pritchard, M. E., & Stewart, A. J. (2016). Recent changes in glacier velocities and thinning at Novaya Zemlya. *Remote Sensing of Environment*, 174, 244–257. <https://doi.org/10.1016/j.rse.2015.11.001>
- Millan, R., Mouginot, J., & Rignot, E. (2017). Mass budget of the glaciers and ice caps of the Queen Elizabeth Islands, Canada, from 1991 to 2015. *Environmental Research Letters*, 12(2), 24,016. <https://doi.org/10.1088/1748-9326/aa5b04>
- Moholdt, G., Wouters, B., & Gardner, A. S. (2012). Recent mass changes of glaciers in the Russian High Arctic. *Geophysical Research Letters*, 39, L10502. <https://doi.org/10.1029/2012GL051466>
- Mortimer, C. A., Sharp, M., & Van Wychen, W. (2018). Influence of recent warming and ice dynamics on glacier surface elevations in the Canadian High Arctic, 1995–2014. *Journal of Glaciology*, 64(245), 450–464.
- Nerem, R., Beckley, B. D., Fasullo, J. T., Hamlington, B. D., Masters, D., & Mitchum, G. T. (2018). Climate-change-driven accelerated sea-level rise detected in the altimeter era. *Proceedings of the National Academy of Sciences*, 115(8), 2022–2025.
- Oleson, K. W., Lawrence, D. M., Bonan, G. B., Drewniak, B., Huang, M., Koven, C., & Yang, Z. L. (2013). Technical description of version 4.5 of the Community Land Model (CLM) (NCAR Technical Note, 503+STR(July)). <https://doi.org/10.5065/D6RR1W7M>
- Paulson, A., Zhong, S., & Wahr, J. (2007). Inference of mantle viscosity from GRACE and relative sea level data. *Geophysical Journal International*, 171(2), 497–508.
- Peltier, W., Argus, D., & Drummond, R. (2015). Space geodesy constrains ice age terminal deglaciation: The global ICE-6G_C (VM5a) model. *Journal of Geophysical Research: Solid Earth*, 120, 450–487. <https://doi.org/10.1002/2014JB011176>
- Raftery, A. E. (1995). Bayesian model selection in social research. *Sociological methodology*, 25, 111–164.
- Reager, J. T., Gardner, A. S., Famiglietti, J. S., Wiese, D. N., Eicker, A., & Lo, M. H. (2016). A decade of sea level rise slowed by climate-driven hydrology. *Science*, 351(6274), 699–703. <https://doi.org/10.1126/science.aad8386>
- Rienecker, M. M., Suarez, M. J., Gelaro, R., Todling, R., Bacmeister, J., Liu, E., et al. (2011). MERRA: NASA's Modern-Era Retrospective Analysis for Research and Applications. *Journal of climate*, 24(14), 3624–3648.
- Rietbroek, R., Brunnabend, S. E., Kusche, J., Schröter, J., & Dahle, C. (2016). Revisiting the contemporary sea-level budget on global and regional scales. *Proceedings of the National Academy of Sciences*, 113(6), 1504–1509. <https://doi.org/10.1073/pnas.1519132113>
- Rodell, M., & Beaudoin, H. (2016). GLDAS Noah Land Surface Model L4 3 hourly 0.25 × 0.25 degree V2.1. <https://doi.org/10.5067/E7TYRXPJKWOQ>
- Rodell, M., Velicogna, I., & Famiglietti, J. S. (2009). Satellite-based estimates of groundwater depletion in India. *Nature*, 460(7258), 999–1002. <https://doi.org/10.1038/nature08238>

- Rui, H., & Beaudoin, H. (2017). README document for NASA GLDAS version 2 data products.
- Rupper, S., Schaefer, J. M., Burgener, L. K., Koenig, L. S., Tsering, K., & Cook, E. R. (2012). Sensitivity and response of Bhutanese glaciers to atmospheric warming. *Geophysical Research Letters*, 39, L19503. <https://doi.org/10.1029/2012GL053010>
- Schrama, E. J. O., Wouters, B., & Rietbroek, R. (2014). A mascon approach to assess ice sheet and glacier mass balances and their uncertainties from GRACE data. *Journal of Geophysical Research: Solid Earth*, 119, 6048–6066. <https://doi.org/10.1002/2013JB010923>
- Sørensen, L. S., Jarosch, A. H., Aðalgeirsdóttir, G., Barletta, V. R., Forsberg, R., Pálsson, F., & Jóhannesson, T. (2017). The effect of signal leakage and glacial isostatic rebound on GRACE-derived ice mass changes in Iceland. *Geophysical Journal International*, 209(1), 226–233. <https://doi.org/10.1093/gji/ggx008>
- Sutterley, T. C., & Velicogna, I. (2019). Improved estimates of geocenter variability from time-variable gravity and ocean model outputs. *Remote Sensing*, 11(18), 2108.
- Tapley, B. D., Bettadpur, S., Watkins, M., & Reigber, C. (2004). The gravity recovery and climate experiment: Mission overview and early results. *Geophysical Research Letters*, 31, L09607. <https://doi.org/10.1029/2004GL019920>
- Tapley, B. D., Watkins, M. M., Flechtner, F., Reigber, C., Bettadpur, S., Rodell, M., et al. (2019). Contributions of GRACE to understanding climate change. *Nature climate change*, 9, 358.
- Tedesco, M., & Fettweis, X. (2020). Unprecedented atmospheric conditions (1948–2019) drive the 2019 exceptional melting season over the Greenland ice sheet. *The Cryosphere Discussions*, 14, 1209–1223. <https://doi.org/10.5194/tc-2019-254>
- Tiwari, V. M., Wahr, J., & Swenson, S. (2009). Dwindling groundwater resources in northern India, from satellite gravity observations. *Geophysical Research Letters*, 36, L18401. <https://doi.org/10.1029/2009GL039401>
- Vaughan, D., Comiso, J., Allison, I., Carrasco, J., Kaser, G., Kwok, R., & Zhang, T. (2013). Observations: Cryosphere. *Climate Change 2013: The Physical Science Basis. Contribution of Working Group I to the Fifth Assessment Report of the Intergovernmental Panel on Climate Change* (pp. 317–382). <https://doi.org/10.1017/CBO9781107415324.012>
- Velicogna, I., & Wahr, J. (2013). Time-variable gravity observations of ice sheet mass balance: Precision and limitations of the GRACE satellite data. *Geophysical Research Letters*, 40, 3055–3063. <https://doi.org/10.1002/grl.50527>
- Weisberg, S. (2005). *Applied linear regression*, (Vol. 528). Hoboken, NJ: John Wiley & Sons.
- Willis, M., Melkonian, A. K., Pritchard, M. E., & Rivera, A. (2012). Ice loss from the Southern Patagonian Ice Field, South America, between 2000 and 2012. *Geophysical Research Letters*, 39, 17. <https://doi.org/10.1029/2012GL053136>
- Wouters, B., & Moholdt, G. (2019). Global glacier mass loss during the GRACE satellite mission (2002–2016), 1–11, pp. Gardner, A. S.
- Yao, T., Thompson, L., Yang, W., Yu, W., Gao, Y., Guo, X., & Joswiak, D. (2012). Different glacier status with atmospheric circulations in Tibetan Plateau and surroundings. *Nature Climate Change*, 2(9), 663–667. <https://doi.org/10.1038/nclimate1580>
- Zhan, J., Shi, H., Wang, Y., & Yao, Y. (2017). Complex principal component analysis of mass balance changes on the Qinghai–Tibetan Plateau. *The Cryosphere*, 11(3), 1487–1499. <https://doi.org/10.5194/tc-11-1487-2017>
- Zhao, M., Ramage, J., Semmens, K., & Obleitner, F. (2014). Recent ice cap snowmelt in Russian High Arctic and anti-correlation with late summer sea ice extent. *Environmental Research Letters*, 9(4), 45,009. Retrieved from <http://stacks.iop.org/1748-6909326/9/i=4/a=045009>
- Zuo, Z., & Oerlemans, J. (1997). Contribution of glacier melt to sea-level rise since AD 1865: A regionally differentiated calculation. *Climate Dynamics*, 13(12), 835–845. <https://doi.org/10.1007/s003820050200>

Erratum

In the originally published version of this article, the last sentence of the Plain Language Summary contained an error. The phrase “an extra 1.4-mm sea level rise” has since been corrected to read “an extra 0.14-mm sea level rise.” This corrected version may be considered the authoritative version of record.